Minerals Engineering 227 (2025) 109278

Contents lists available at ScienceDirect

Minerals Engineering

journal homepage: www.elsevier.com/locate/mineng

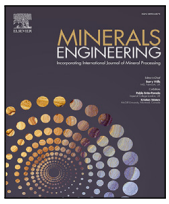

Model-plant mismatch diagnosis using plant model ratios for a grinding mill circuit under model predictive control

Heinz K. Mittermaier [a,b], Johan D. le Roux [b,*], Ian K. Craig [b]

[a] Measurement and Control Division, Mintek, Johannesburg, South Africa
[b] Department of Electrical, Electronic, and Computer Engineering, University of Pretoria, Pretoria, South Africa

ARTICLE INFO

Keywords:
Controller performance monitoring
Grinding mill circuit
Model predictive control
Model-plant mismatch
Process performance monitoring

ABSTRACT

Model-based controllers often extend improved performance to mineral processing plants by leveraging predictive models to account for system dynamics, handling constraints, adapting to changing conditions, and optimizing control inputs. Inaccurate models will cause a deterioration of controller performance, which is often the case for grinding mill circuits. The plant model ratio was developed to diagnose parametric model plant mismatches for first-order plus time delay models. Using a simulation study, the plant model ratio is applied to test the feasibility of using the plant model ratio on a grinding mill circuit. By applying different scenarios of mismatch, some limitations of the plant model ratio are identified and discussed in light of a grinding mill circuit model that is used in model-based controllers. The plant model ratio is capable of identifying parametric model plant mismatches for the model of a grinding mill circuit, specifically changes in the direction of responses. This may occur in cases where disturbances push a grinding mill to operate to the right of the peak of a grind curve.

1. Introduction

Grinding mill circuits are highly interactive systems, have strict process constraints, contain non-linear interactions, and experience frequent disturbances (Le Roux and Craig, 2019). Model-based controllers such as model-predictive control (MPC) provide significant advantages over proportional–integral–derivative (PID) controllers to maintain the process at the desired operating condition despite these challenges (Remes et al., 2010; Ramasamy et al., 2005; Pomerleau et al., 2000).

Grind curves are quazi-stationary parabolic curves that relate the mill filling to performance indicators such as power draw, throughput and product size (Powell et al., 2009; Le Roux et al., 2020). In general, the aim is to operate at a mill filling close to the peak of the throughput grind curve, which is usually left of the peak of the power grind curve (Craig et al., 1992). Disturbances such as feed ore hardness or particle size distribution (Morrell et al., 1996) may cause the grind curves to shift such that the process operates to the right of the grind curves. This may result in an inversion of the direction of the relationship between mill filling and power draw, throughput, or product size (Steyn et al., 2010).

System identification is often used to derive linear time-invariant (LTI) transfer function models for use in linear MPC. For grinding mills, the sign of the gain of an LTI model between two process variables may change depending on which side of the grind curve the system is operating. Since a change in process dynamics is unavoidable because of process disturbances, the accuracy of the model used for an MPC controller of a grinding mill may deteriorate over time (Olivier and Craig, 2013). The deterioration of model accuracy, i.e., model-plant mismatch (MPM), is a common problem for MPC (Qin and Badgwell, 2003; Mayne, 2014; Schwenzer et al., 2021). This results in a deterioration in the performance of the MPC, and is one of the main impediments to ensure long-term successful implementation of MPC in grinding mill circuits. Subsequently, PID control remains the standard approach to control grinding mill circuits in industry (Wei and Craig, 2009; Hodouin, 2011; Olivier and Craig, 2017).

To address the deterioration of controller performance, a substantial amount of research has been done on the topic of controller performance monitoring (CPM), consisting of several subsets of research. This article will focus on model-plant mismatch (MPM) detection since the focus of the study is on model-based controllers. CPM, in the form of MPM detection and isolation, is categorized into either direct or indirect methods (Wu and Du, 2022).

The principal categories for the indirect methods of MPM are statistical-based techniques and sensitivity function-based methods. Badwe et al. (2009) proposed the first statistical-based technique

* Corresponding author.
E-mail address: derik.leroux@up.ac.za (J.D. le Roux).

https://doi.org/10.1016/j.mineng.2025.109278
Received 12 February 2024; Received in revised form 17 February 2025; Accepted 25 March 2025
Available online 7 April 2025

derived from a partial correlation analysis on which most of the statistical-based methodologies are developed. The proposed methodology first calculates the disturbance-free components of the manipulated variable (MV). These disturbance-free MV components are decorrelated to all other MVs ($\hat{\epsilon}_{u_i}$) to allow a single transfer function containing the MPM to be identified within a multiple-input–multiple-output (MIMO) transfer function matrix. The same steps are used to decorrelate the model residuals to all the MVs ($\hat{\epsilon}_{e_j}$). A non-zero cross-correlation between $\hat{\epsilon}_{u_i}$ and $\hat{\epsilon}_{e_j}$ indicates an MPM within the $u_i - y_j$ input–output channel, where u_i is the ith input and y_j is the jth output of the system. The larger the correlation coefficient the more significant the MPM will be.

In contrast to the required setpoint excitation of the partial correlation analysis developed by Badwe et al. (2009), the correlation analysis method described by Li et al. (2020) requires a data set with zero setpoint changes. The methodology uses a correlation analysis method between the inputs and the disturbances along with a model quality index to formulate a custom model assessment index applicable to an MPC algorithm using a univariate predictive control structure.

In addition to using a partial correlation, other statistical-based techniques include the plant model ratio (PMR) as developed by Selvanathan and Tangirala (2010a). The PMR is defined as the ratio of the plant transfer function to the model transfer function. This definition of MPM allows for the diagnosis of gain, time-constant and delay mismatches within a single-input and single-output (SISO) system, with the caveat that high-frequency broadband excitation is required within the system. To mitigate the requirement for high-frequency excitation, an improved PMR method, as described by Yerramilli and Tangirala (2018), was developed where an optimal delay estimation technique is used to allow for delay mismatch diagnosis without high-frequency excitation. Selvanathan and Tangirala (2010a) discussed how to estimate the PMR from routine operational data while Yerramilli and Tangirala (2016) expanded the PMR estimation to MIMO systems by introducing a decoupling estimation of the PMR for multivariable systems.

The variance ratio-based model evaluation index, much like the partial correlation analysis (Badwe et al., 2009) and the PMR (Selvanathan and Tangirala, 2010a), is based on the internal model control (IMC) structure. This method of MPM detection uses the adaptive Lasso approach to determine the order and estimate the parameters of a linear regression model (Zou, 2006).

In light of the discussion above, the PMR shows the potential to not only identify MPM, but also isolate the MPM to a specific input–output model within the MIMO transfer function matrix. It can also identify the type of mismatch as either gain-, dynamic–, or delay mismatch and give a diagnosis of the direction of each mismatched parameter.

To enable long-term use of MPC for grinding mill circuits, this article investigates the applicability of the PMR as a method to identify MPM in a grinding mill circuit. This is a continuation of the study in Mittermaier et al. (2023). However, here an improved PMR approach is used, the ability to identify an inversion in polarity of process gains is investigated, and conditions for the successful use of PMR is shown.

The article is structured as follows. Section 2 summarizes the PMR approach of Selvanathan and Tangirala (2010a), as well as the improved PMR by Yerramilli and Tangirala (2018). Section 3 gives the LTI model obtained by system identification of a non-linear grinding mill circuit model (Ziolkowski et al., 2022). Section 4 simulates MPM for the circuit using an uncertainty description (Craig and MacLeod, 1995) and presents the results of applying PMR. Section 5 discusses the challenges of using PMR to identify MPM for a grinding mill circuit.

2. Plant model ratio

The IMC structure is shown in Fig. 1, where $R(\omega)$ is the reference signal, $U(\omega)$ is the control input, $V(\omega)$ is the measurement noise, $Y(\omega)$ is the plant output, $\hat{Y}(\omega)$ is the model output, and $E(\omega)$ is the error signal. A frequency domain representation of all the variables is given.

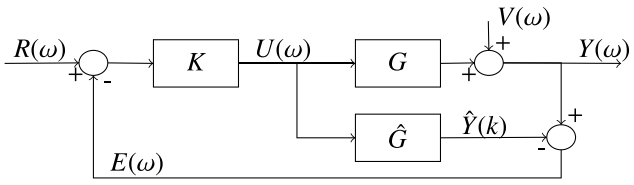

Fig. 1. Closed-loop IMC structure.

The IMC structure allows for model-plant comparison by investigating the difference between the plant (G) and an online version of the plant model ($\hat{G}$). This comparison denotes the traditional form of MPM and can be represented as $\Delta G = G - \hat{G}$. Since ΔG is seldom zero, due to modeling uncertainties and the lack of accurate process knowledge, the PMR was developed to mitigate the shortcomings of the traditional MPM (ΔG) and provide a method to collect more information on MPM.

The objective of the PMR for SISO systems, as developed by Selvanathan and Tangirala (2010a), is to recognize, isolate, and diagnose the MPM by categorizing it as a gain mismatch, delay mismatch, dynamic mismatch, or a combination of these three mismatch types.

2.1. Plant model ratio for SISO systems

From Fig. 1, the PMR is defined as the ratio of the frequency response function of the plant ($G(e^{j\omega})$) to the frequency response function of the model ($\hat{G}(e^{j\omega})$) (Yerramilli and Tangirala, 2016),

$$G_{PMR}(e^{j\omega}) = \frac{G(e^{j\omega})}{\hat{G}(e^{j\omega})}. \tag{1}$$

The polar representation of (1) is,

$$\begin{aligned} G_{PMR}(e^{j\omega}) &= \frac{|G(e^{j\omega})|e^{j\angle \underline{G}(e^{j\omega})}e^{-jD\omega}}{|\hat{G}(e^{j\omega})|e^{j\angle \underline{\hat{G}}(e^{j\omega})}e^{-j\hat{D}\omega}} \\ &= M(\omega)e^{j\Delta P(\omega)}, \end{aligned} \tag{2}$$

where $\underline{G}$ and $\underline{\hat{G}}$ represent the delay-free parts of the plant and the model transfer functions, respectively. D refers to the delay present in the system. Instead of analyzing ΔG, as done in most MPM approaches, (2) evaluates the ratio of the mismatch in magnitude $M(\omega) = \frac{|G(e^{j\omega})|}{|\hat{G}(e^{j\omega})|}$ and phase $\Delta P(\omega) = \frac{e^{j\angle \underline{G}(e^{j\omega})}e^{-jD\omega}}{e^{j\angle \underline{\hat{G}}(e^{j\omega})}e^{-j\hat{D}\omega}}$.

Selvanathan and Tangirala (2010a) developed a systematic approach, applying the PMR to first-order plus time-delay (FOPTD) models, e.g., the plant is defined as $G(s) = \frac{K}{\tau s+1}e^{-Ds}$, and the plant model as $\hat{G}(s) = \frac{\hat{K}}{\hat{\tau}s+1}e^{-\hat{D}s}$, in order to diagnose the MPM present in the system. The approach includes the analysis of the zero-frequency component of the magnitude spectrum of the PMR to determine the gain mismatch. This is followed by a test of the slope of the magnitude spectrum of the PMR to ascertain the extent of the dynamic mismatch present, and lastly, a linearity check of the phase spectrum of the PMR is used to diagnose the delay mismatch present (Selvanathan and Tangirala, 2010a; Yerramilli and Tangirala, 2016). The full systematic diagnosis procedure is captured in Table 1. In Step 1, if $M(\omega)$ evaluated at $\omega = 0$ is not equal to 1, there is a mismatch in the steady-state gain (K). If $M(\omega = 0) > 1$, the plant gain K is greater than the model gain $\hat{K}$, if $M(\omega = 0) < 1$, the plant gain K is less than the model gain $\hat{K}$. In Step 2, the initial slope of the magnitude spectrum is used to determine the extent of the time-constant mismatch. If the slope is greater than 0, the plant time-constant (τ) is less than the model time-constant ($\hat{\tau}$), if the slope is less than 0, the plant time-constant (τ) is greater than model time-constant ($\hat{\tau}$). The last step, Step 3, is to do a linearity check on the entire phase spectrum. This can be done by fitting a linear line to the phase spectrum and using the slope of the fitted line, α to determine the phase linearity. If the phase spectrum increases over frequency then the plant delay (D) is less than the model delay ($\hat{D}$), and if the phase spectrum decreases over frequency then the plant delay (D) is greater than the model delay ($\hat{D}$).

Table 1
MPM analysis using PMR.

	Assessment procedure	Diagnosis of MPM	MPM direction
Step 1	$M(\omega)\|_{\omega=0} \neq 1$	if $M(0) = 1$: $K = \hat{K}$, else $K \neq \hat{K}$	$M(\omega) > 1$ if $K > \hat{K}$, $M(\omega) < 1$ if $K < \hat{K}$
Step 2	$M(\omega)$ has a zero slope (flatness test)	if flat: $\tau = \hat{\tau}$, else $\tau \neq \hat{\tau}$	$M(\omega)\|_{\omega=\pi} < 1$ if $\tau > \hat{\tau}$, $M(\omega)\|_{\omega=\pi} > 1$ if $\tau < \hat{\tau}$
Step 3	Linearity check of $\Delta P(\omega)$	if $\alpha = 0$: $D = \hat{D}$, else $D \neq \hat{D}$	$\alpha > 0$ if $D < \hat{D}$, $\alpha < 0$ if $D > \hat{D}$

Table 2
MPM analysis using improved PMR.

	Assessment procedure	Diagnosis of MPM	MPM direction
Step 1	$M(\omega)\|_{\omega=0} \neq 1$	if $M(0) = 1$: $K = \hat{K}$, else $K \neq \hat{K}$	$M(\omega) > 1$ if $K > \hat{K}$, $M(\omega) < 1$ if $K < \hat{K}$
Step 2	$M(\omega)$ has a zero slope (flatness test)	if flat: $\tau = \hat{\tau}$, else $\tau \neq \hat{\tau}$	$M(\omega)\|_{\omega=\pi} < 1$ if $\tau > \hat{\tau}$, $M(\omega)\|_{\omega=\pi} > 1$ if $\tau < \hat{\tau}$
Step 3	Optimal delay mismatch detection		

2.2. Plant model ratio estimation for SISO systems

As seen in (1), the PMR is defined as the ratio between the process transfer function G and the model transfer function $\hat{G}$. Due to process variation and non-linearity most process transfer functions will not be known apriori. To address this issue, the PMR can under certain conditions be estimated from routine operating data. These conditions include that the setpoint contains sufficient excitation and that the signal-to-noise ratio is large enough to make reliable inferences (Yerramilli and Tangirala, 2018).

The cross-spectral density (CSD) is used to estimate the PMR (Ljung, 1999; Selvanathan and Tangirala, 2010a),

$$\hat{G}_{PMR} = \frac{\gamma_{y,r}(\omega)}{\gamma_{\hat{y},r}(\omega)}, \tag{3}$$

where $\gamma_{y,r}(\omega)$ is the estimated CSD between the plant output y and the setpoint r, while $\gamma_{\hat{y},r}(\omega)$ is the estimated CSD between the model output $\hat{y}$ and the setpoint r. This correlation between outputs and setpoint allows for the effects of noise and disturbances (which should be uncorrelated with the setpoint) to be removed from the estimate of the PMR (Selvanathan and Tangirala, 2010a; Yerramilli and Tangirala, 2016).

From the polar representation of the PMR in (2), two pitfalls should be avoided (Mittermaier et al., 2023),

1. Since the PMR is based on a frequency analysis, sufficient broadband setpoint excitation is required. For example, a sinusoid of a single frequency will excite a LTI system only at that frequency, which will lead to a lack of information at other frequencies that may be of interest in the CSD (Priestley, 1981).
2. If the model used to describe the system is not a deviation variable model (Skogestad and Postlethwaite, 2010), the operating point of each variable of the system should be subtracted from the recorded data. Eliminating the offset in the data will remove the corresponding lower frequency components that will otherwise dominate the CSD and ensure accurate results for the PMR.

2.3. The improved plant model ratio

The delay mismatch detection seen in Table 1 requires high-frequency excitation to estimate the delay mismatch (Mittermaier et al., 2023; Selvanathan and Tangirala, 2010a; Yerramilli and Tangirala, 2016). This requirement is undesirable in real-world systems due to the effect of high-frequency signals on plant actuators as well as the low-pass filtering effect of feedback control systems. Therefore, to mitigate this requirement, an improved PMR methodology was developed by estimating the delay mismatch using optimal delay estimation (Hamon and Hannan, 1974; Lindemann et al., 2001; Selvanathan and Tangirala, 2010b).

An arbitrary transfer function $H(\omega)$ can be split into a transfer function containing the delay-free portion of the system ($\underline{H}(\omega)$) and the delay of the system ($e^{-D\omega}$),

$$H(\omega) = \underline{H}(\omega)e^{-D\omega}. \tag{4}$$

The phase spectrum of the transfer function contains a contribution from both the time-delay and delay-free part of the transfer function,

$$\arg[H(\omega)] = \arg[\underline{H}(\omega)] - D(\omega), \tag{5}$$

where arg represents the angle of the complex number. Therefore, if the left-hand side and the delay-free contribution of (5) is known, the delay (D) can be estimated. The left-hand side of (5) can be estimated, by using the linear system relation,

$$H(\omega) = \frac{\gamma_{yu}(\omega)}{\gamma_{uu}(\omega)}, \tag{6}$$

where $\gamma_{yu}(\omega)$ is the CSD between the input and output of the system, and $\gamma_{uu}(\omega)$ is the auto-spectral-density of the system input.

Note the magnitude of the delay-free term ($\underline{H}(\omega)$) and the magnitude of the complete transfer function ($H(\omega)$) in (5) are identical, i.e., $|H(\omega)| = |\underline{H}(\omega)|$. Therefore, $arg[\underline{H}(\omega)]$ can be estimated as shown in (7), without using the delay factorization in (4). Assuming that $H(\omega)$ is a minimum phase system, $arg(\underline{H}(\omega))$ in (5) can be approximated using a discretized Hilbert transform relation (Oppenheim, 1999),

$$\arg\left[\underline{H}\left(\omega_l\right)\right] = -\frac{1}{2B}\sum_{k=1,k\neq l}^{B} \log\left|H\left(\omega_k\right)\right| \left(\cot\left(\frac{\omega_l - \omega_k}{2}\right) + \cot\left(\frac{\omega_l + \omega_k}{2}\right)\right), \tag{7}$$

where, ω_l is the frequency in question, while ω_k forms a moving window of frequencies within a bandwidth of frequencies denoted by B (Lindemann et al., 2001).

The estimates of $\arg[H(\omega)]$ as in (6), and $\arg[\underline{H}(\omega)]$ as in (7) can be substituted into (5) to form the following error function,

$$\epsilon(\omega) = \arg[\hat{H}(\omega)] - \arg[\underline{\hat{H}}(\omega)] + D(\omega). \tag{8}$$

From the error function the delay (D) can be determined by solving the cost function (Hamon and Hannan, 1974),

$$\max_D J(D) = \sum_B W(\omega)\cos(\epsilon(\omega)), \tag{9}$$

where W is the weighting function as defined in (11).

When the error term of (8) tends to zero, the cosine function in (9) will reach a peak value. Therefore, the cost function searches for the integer value of D that realizes the maximum value of the cost function over the same bandwidth, B, as in (7). The bandwidth is a proper band of normalized frequencies $[0, \pi/T_s]$, where T_s is the sampling rate.

The weighting function of the objective function is derived from a least-squares approach (Ljung, 1999) with the aim of applying a bias to the objective function that is inversely proportional to the variance of the phase spectral estimate per normalized frequency. When using

the smoothed periodogram method to estimate the phase spectra, the variance of the phase estimate will be (Lindemann et al., 2001),

$$\mathrm{var}(\arg[\hat{H}(\omega)]) = \frac{1}{\nu}\left(\frac{1}{\kappa^2(\omega)} - 1\right), \tag{10}$$

where ν is the degrees of freedom and $\kappa^2(\omega)$ is the magnitude-squared coherence between the input and output of the system. The weighting function $W(\omega)$ is therefore chosen based on the weighted least-squares as,

$$W(\omega) = \frac{\kappa^2(\omega)}{1-\kappa^2(\omega)}. \tag{11}$$

Combining the weighting function in (11) with the error function in (8) and the objective function in (9), a non-linear integer optimization problem should be solved to estimate the delay D. Seeing that in an actual real-world process, the expected delay variability due to MPM tends to be small, the non-linear integer optimization can be simplified to a standard search over a predetermined variable set of plausible integers, for example, $D \in \mathbb{Z}|_{-10\leq D\leq 10}$.

From the assumption that the PMR can be represented as a transfer function between the process output (y) and the model output ($\hat{y}$), as mentioned by Yerramilli and Tangirala (2016), the arbitrary transfer function ($H(\omega)$) can directly be replaced with the PMR (G_{PMR}) to obtain the MPM within the delay term of the transfer function in question. The last step of Table 1 can thus directly be replaced with the optimal delay estimation, as seen in Table 2.

2.4. Plant model ratio expanded to MIMO systems

For a MIMO system, the matrix elements are SISO transfer functions between individual input/output channels,

$$\mathbf{G} = \begin{bmatrix} G_{11} & G_{12} & \cdots & G_{1j} \\ G_{21} & G_{22} & \cdots & G_{2j} \\ \vdots & \vdots & \ddots & \vdots \\ G_{i1} & G_{i2} & \cdots & G_{ij} \end{bmatrix}. \tag{12}$$

The objective of the PMR when applied to a MIMO system would be to isolate the MPM to a specific transfer function within the MIMO transfer function matrix and apply the SISO PMR diagnosis procedure (Table 2) to each element in the matrix. Seeing that the SISO PMR, as described in (1), cannot be directly applied to MIMO systems in a trivial way, an approach to the MIMO PMR was developed by Yerramilli and Tangirala (2016). From the IMC structure in Fig. 1, the plant output Y_i can be expressed in terms of the model output $\hat{Y}_i$,

$$\begin{aligned} Y_i(\omega) &= \sum_{k=1}^{n} G_{ik}(\omega)U_k(\omega) + V_i(\omega) \\ &= \sum_{k=1}^{n} G_{PMR_{ik}}(\omega)\hat{G}_{ik}(\omega)U_k(\omega) + V_i(\omega) \\ &= \sum_{k=1}^{n} G_{PMR_{ik}}(\omega)\hat{y}_{ik}(\omega) + V_i(\omega), \end{aligned} \tag{13}$$

where $\hat{Y}_{ik}$ is the kth component, of the ith model output ($\hat{Y}_i$), corresponding to the kth input u_k. Thus, for an $n \times n$ MIMO system, the element-wise division between the plant and model transfer function matrices defines the PMR matrix (Yerramilli and Tangirala, 2016, 2018),

$$\begin{aligned} \mathbf{G}_{PMR}(\omega) &= \begin{bmatrix} \frac{G_{11}(\omega)}{\hat{G}_{11}(\omega)} & \cdots & \frac{G_{1n}(\omega)}{\hat{G}_{1n}(\omega)} \\ \vdots & \ddots & \vdots \\ \frac{G_{n1}(\omega)}{\hat{G}_{n1}(\omega)} & \cdots & \frac{G_{nn}(\omega)}{\hat{G}_{nn}(\omega)} \end{bmatrix} \\ &= \begin{bmatrix} G_{PMR_{11}} & \cdots & G_{PMR_{1j}} \\ \vdots & \ddots & \vdots \\ G_{PMR_{i1}} & \cdots & G_{PMR_{ij}} \end{bmatrix}. \end{aligned} \tag{14}$$

2.4.1. MIMO PMR estimation from operational data

As discussed in Section 2.2, the process transfer function will seldom be known apriori, thus, the MIMO PMR must be estimated using routine operational data. If the inputs are uncorrelated, i.e., the transfer function matrix of (12) is a diagonal matrix, the PMR can be described as (Yerramilli and Tangirala, 2016, 2018),

$$G_{PMR_{ij}}(\omega) = \frac{\gamma_{y_i,\hat{y}_{ij}}(\omega)}{\gamma_{\hat{y}_{ij},\hat{y}_{ij}}(\omega)}, \tag{15}$$

where the ith row of the PMR matrix in (14) is interpreted as a transfer function between the n components of the model output $\hat{y}_i$ and the plant output y_i.

Since MIMO industrial systems typically do not have a diagonal transfer function matrix and significant correlations exist between all inputs and all outputs, the PMR in (15) does not hold true due to the confounding effect, i.e., the PMR in a particular channel is also influenced by contributions of inputs/outputs from other channels (Yerramilli and Tangirala, 2018).

The confounding effect between correlated channels can be mitigated using either an implicit or explicit MIMO PMR estimation. The explicit method of estimating the MIMO PMR uses a partial CSD (Yerramilli and Tangirala, 2016). The implicit method, which is simpler than the explicit method, will be used in this article and is described in Section 2.4.2.

2.4.2. Implicit MIMO PMR estimation

The implicit method of estimating the PMR uses a multiple regression approach on (13) by firstly correlating both sides of the equation with all setpoints. The correlation realizes n equations for n entries of each row of the MIMO PMR matrix as seen in (16). The correlation step mitigates the effects of disturbances and noise (Yerramilli and Tangirala, 2018).

$$\begin{bmatrix} \gamma_{y_i,r_1}(\omega) \\ \gamma_{y_i,r_2}(\omega) \\ \vdots \\ \gamma_{y_i,r_n}(\omega) \end{bmatrix} = \begin{bmatrix} \gamma_{\hat{y}_{i1},r_1}(\omega) & \cdots & \gamma_{\hat{y}_{in},r_1}(\omega) \\ \gamma_{\hat{y}_{i1},r_2}(\omega) & \cdots & \gamma_{\hat{y}_{in},r_2}(\omega) \\ \vdots & \ddots & \vdots \\ \gamma_{\hat{y}_{i1},r_n}(\omega) & \cdots & \gamma_{\hat{y}_{in},r_n}(\omega) \end{bmatrix} \begin{bmatrix} G_{PMR_{i1}}(\omega) \\ G_{PMR_{i2}}(\omega) \\ \vdots \\ G_{PMR_{in}}(\omega) \end{bmatrix} \tag{16}$$

Therefore, elements of the ith row of the PMR matrix can be estimated via regression. It should be noted that the values in (16) are complex, and therefore the complex conjugate transpose operation should be used for each frequency within the bandwidth B when calculating the $G_{PMR_{ij}}$ values (Yerramilli and Tangirala, 2018).

The implicit method of estimating the PMR matrix realizes a matrix of SISO PMR transfer functions, homogeneous to the SISO PMR transfer function in (3). Therefore, the SISO analysis and systematic diagnosis shown in Table 2 can be applied to each entry of the PMR matrix.

2.4.3. Importance of scaling

As shown in (16), each individual model output is used to decouple the process outputs from the PMR matrix. Therefore, attention should be given to the relative size difference in gain terms of each transfer function within the transfer function matrix (Skogestad and Postlethwaite, 2010). These size differences in gain terms can cause an overpowering of information within the frequency analysis, most prominently in the CSD calculation (Lathi and Ding, 2010; Proakis and Salehi, 2014).

As seen in (3), the PMR is estimated as a ratio of two CSDs ($\hat{G}_{PMR} = \frac{\gamma_{y,r}(\omega)}{\gamma_{\hat{y},r}(\omega)}$) and the estimation of the MIMO PMR includes a ratio of CSDs between all process outputs and model outputs in (16).

Considering the mathematical formulation of the CSD (Oppenheim, 1999), $P_{xy}(\omega) = \sum_{m=-\infty}^{\infty} R_{xy}(m)e^{-j\omega m}$, where R_{xy} is the cross-correlation sequence between signals x and y, defined as, $R_{xy}(m) = E\left\{x_{n+m}y_n^*\right\} = E\left\{x_n y_{n-m}^*\right\}$, the trivial connection between the absolute size of the signals (x and y) and the absolute size of the CSD can be made.

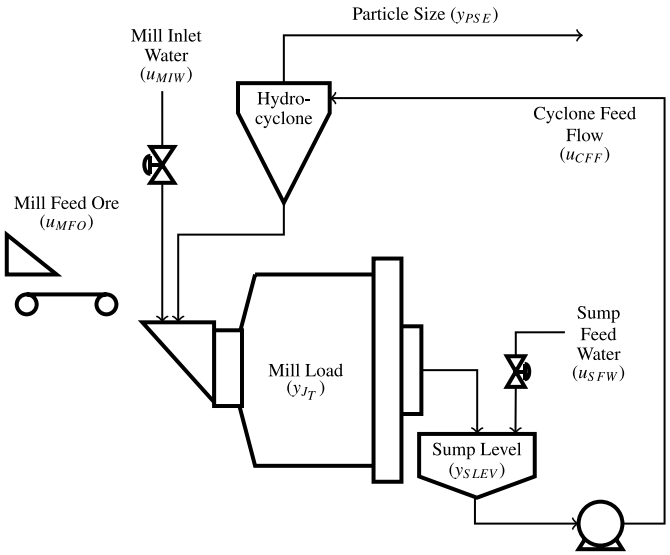

Fig. 2. Single-stage closed grinding mill circuit.

Applying this deduction to the CSD of the MIMO PMR estimation, it is evident that if the plant being diagnosed does not have gains within the same order, the ratio of the PMR ($\hat{G}_{PMR} = \frac{\hat{\gamma}_{y,r}(\omega)}{\hat{\gamma}_{\hat{y},r}(\omega)}$) might be overpowered by model outputs having a different output size (larger or smaller) when compared to the plant output size.

This limitation of the PMR can be accounted for by normalizing the gain values of all transfer functions within the MIMO transfer function of the plant under consideration (Skogestad and Postlethwaite, 2010).

3. Grinding mill

The PMR is used to identify MPM in the LTI model representation of a grinding mill circuit. A semi-autogenous grinding (SAG) mill circuit is used as the case study.

The SAG mill in Fig. 2 receives the mined ore to be milled (u_{MFO}), along with water, steel balls, and the underflow of the hydrocyclone to form the mill load (y_{J_T}). The mill turns causing the falling balls to crush the ore and mix the broken ore in the mill to form a slurry. An end-discharge grate is placed at the outflow of the mill to ensure only the slurry is discharged to the sump. The sump level (y_{SLEV}) is controlled by adding water (u_{SFW}) to the sump. The slurry is pumped from the sump to the hydrocyclone classifier via a variable speed pump to manipulate the cyclone feed flow rate (u_{CFF}). The hydrocyclone classifier allows fine ore in the slurry to exit the circuit via the hydrocyclone overflow, while the coarse ore returns to the mill for further grinding via the hydrocyclone underflow. The percentage of ore particles in the overflow below a specification size is defined as y_{PSE}.

The mill is modeled as in Ziolkowski et al. (2022), using an adapted version of the continuous-time phenomenological non-linear population balance model of Le Roux et al. (2020) and Le Roux and Steyn (2022). The developed model provides a wide variety of suitable operating conditions based on grind curves to test the MPM diagnosis.

3.1. Linear model fitting

Standard SID procedures, as described by Ljung (1999), can be applied to the non-linear grinding mill circuit by exciting the following three manipulated variables (MVs)

- Cyclone Feed Flow (u_{CFF})
- Mill Feed Ore (u_{MFO})
- Sump Feed Water (u_{SFW})

and measuring the following three controlled variables (CVs)

- Particle Size (y_{PSE})
- Mill Load (y_{J_T})
- Sump Fill (y_{SLEV})

to obtain the model of the grinding mill circuit. The transfer function entries in the MIMO matrix conform to the FOPTD structure, except G_{22}, which is modeled as a pure integrator with a time delay,

$$\begin{bmatrix} y_{PSE} \\ y_{J_T} \\ y_{SLEV} \end{bmatrix} = G \begin{bmatrix} u_{CFF} \\ u_{MFO} \\ u_{SFW} \end{bmatrix}, \tag{17a}$$

where,

$$G = \begin{bmatrix} \frac{-9.9\times10^{-5}e^{-0.044s}}{0.49s+1} & \frac{-5.2\times10^{-4}}{0.19s+1} & \frac{1.9\times10^{-4}}{0.048s+1} \\ \frac{4.3\times10^{-4}}{0.32s+1} & \frac{2.8\times10^{-4}e^{-0.047s}}{s} & \frac{-3.1\times10^{-4}e^{-0.053s}}{0.24s+1} \\ \frac{-45}{53s+1} & \frac{113e^{-0.03s}}{8.3s+1} & \frac{92}{94s+1} \end{bmatrix}. \tag{17b}$$

3.2. Linear model scaling

Since the transfer function matrix in (17) consists of LTI transfer functions, the homogeneity property of an LTI system can be used to scale the plant model in (17). The following scaling matrices were derived from the constraints and operating points as described by Coetzee et al. (2010). The MV scaling matrix ($u_{scaling}$) and the CV scaling matrix ($y_{scaling}$) is,

$$u_{scaling} = \begin{bmatrix} 150 & 0 & 0 \\ 0 & 326 & 0 \\ 0 & 0 & 372.8 \end{bmatrix} \tag{18a}$$

$$y_{scaling} = \begin{bmatrix} 0.015 & 0 & 0 \\ 0 & 0.02 & 0 \\ 0 & 0 & 25 \end{bmatrix}. \tag{18b}$$

The multivariable plant in (17) can be scaled as follows (Skogestad and Postlethwaite, 2010),

$$\begin{aligned} G_{\text{scaled}} &= y_{scaling}^{-1} \times G \times u_{scaling} \\ &= \begin{bmatrix} \frac{200}{3} & 0 & 0 \\ 0 & 50 & 0 \\ 0 & 0 & 0.04 \end{bmatrix} G \begin{bmatrix} 150 & 0 & 0 \\ 0 & 326 & 0 \\ 0 & 0 & 372.8 \end{bmatrix}. \end{aligned} \tag{19}$$

4. Simulation case study

Three scenarios are simulated to test the PMR methodology:

Scenario 1:	PMR is used to detect only gain mismatches applied to the system.
Scenario 2:	An uncertainty description is used to simulate the extent to which MPM can be expected from an industrial grinding mill.
Scenario 3:	A change in sign for transfer functions G_{11} and G_{22}.

4.1. Simulation description

The simulation of the plant was done using the system given in Fig. 3. Both the plant and model outputs are logged for use with the PMR algorithm along with the setpoints. As typically required for model-based control, the CVs of the plant are used in conjunction with a Kalman filter to estimate the plant states. The estimated states along with the required setpoints are fed back into the MPC to determine the required MVs applied to both the model and the plant.

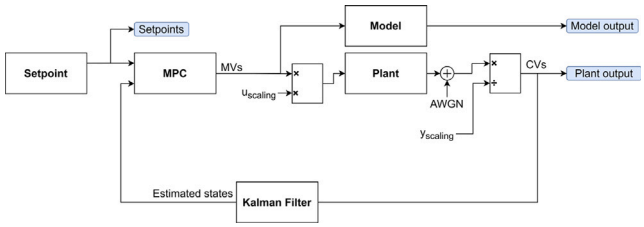

Fig. 3. Grinding mill feedback loop.

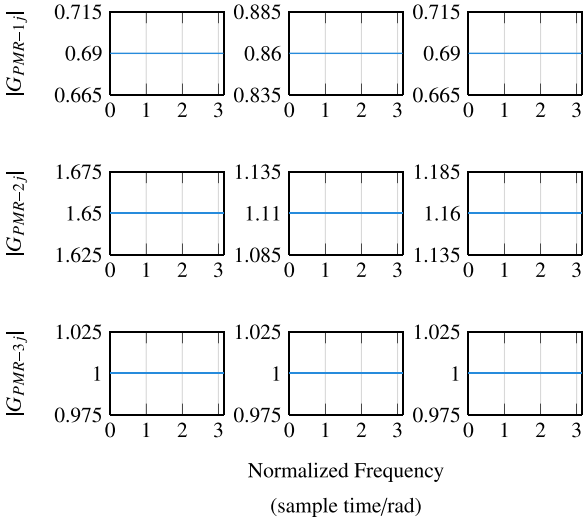

Fig. 4. PMR magnitude spectra for Scenario 1.

To ensure that the necessary excitation is applied to the process, pseudo-random binary sequences, with a maximum switching time of 10 times the sampling rate of 10 s, are used as reference signals. All setpoints are perturbed at the same time. If perturbations are applied to one setpoint at a time, the low-frequency interference to the CSD as described in Section 2.1 is observed. White Gaussian noise (AWGN) is added to the plant outputs to simulate measurement noise.

4.2. Controller design

The plant of (17) is controlled using a linear constrained MPC, based on the scaled version of the transfer function, seen in (19).

The plant is discretized using a sampling time of 10 s. The prediction horizon (N_p) is chosen as 50 samples and the control horizon (N_c) is chosen as 10 samples, while $Q = \text{diag}[100, 100, 50]$ and $R = \text{diag}[10, 10, 10]$ for the cost function of the MPC.

4.3. Model plant mismatch applied

The parametric uncertainty description for the grinding mill circuit shown in (20) is based on Craig and MacLeod (1995). The polarity of each quantity indicates either an increase or decrease applied to the parameter during the MPM simulation.

$$K_{ij} = \begin{bmatrix} -31\% & -14\% & -31\% \\ 65\% & 11\% & 16\% \\ - & - & - \end{bmatrix} \tag{20a}$$

$$\tau_{ij} = \begin{bmatrix} -18\% & - & -19\% \\ 40\% & - & 60\% \\ - & - & - \end{bmatrix} \tag{20b}$$

$$D_{ij} = \begin{bmatrix} 27\% & - & - \\ - & - & 43\% \\ - & - & - \end{bmatrix}. \tag{20c}$$

4.4. Scenario 1 — Gain mismatch diagnosis

To determine the effectiveness of the PMR in diagnosing MPM within the gain terms of the transfer function matrix, the first simulation will only include the MPM seen in (20a).

4.4.1. Step 1 — Gain mismatch

The MPM in the gain term of all transfer functions in the transfer function matrix can be determined using the zero-frequency term of the PMR magnitude spectra as seen in Fig. 4.

$$\begin{aligned} \Delta K &= \left(|\mathbf{G_{PMR}}(0)| - 1\right) \times 100 \\ &= \left(\begin{bmatrix} 0.69 & 0.86 & 0.69 \\ 1.65 & 1.11 & 1.16 \\ 1 & 11 & \end{bmatrix} - 1\right) \times 100 \\ &= \begin{bmatrix} -31\% & -14\% & -31\% \\ 65\% & 11\% & 16\% \\ 0\% & 0\% & 0\% \end{bmatrix}. \end{aligned} \tag{21}$$

4.4.2. Step 2 — Time-constant mismatch

The relative time-constant mismatches can be deduced from the linear fitted line (orange line) to the initial slope of the PMR magnitude spectrum as seen in Fig. 5. All terms are multiplied by −1, to eliminate the inverse relationship between the initial slope and the direction of the time-constant MPM, as shown in Table 2.

$$\begin{aligned} \Delta\tau &= \hat{\alpha}_{\mathbf{G_{PMR}}} \times -100 \\ &= \begin{bmatrix} -0.3365 & 0.3814 & 0.4801 \\ -0.0041 & 0.0589 & -0.0107 \\ 0.0084 & 0.0586 & 0.0215 \end{bmatrix} \times 10^{-10} \approx \mathbf{0}, \end{aligned} \tag{22}$$

where $\hat{\alpha}_{\mathbf{G_{PMR}}}$ is the estimated gradient of a linear fitted line to the PMR.

4.4.3. Step 3 — Delay mismatch

Finally, the time delay mismatch can be estimated using the optimal delay estimation technique, described in Section 2.3. The cost function seen in (9) is solved for all entries in the PMR matrix as seen in Fig. 6. Since the maximum of the cost function results in the delay present in the specific transfer function, from Fig. 6 it is evident that all transfer functions have no MPM since the maximum values calculated for each cost function is at $D = 0$.

$$\Delta D = \begin{bmatrix} 0 \text{ samples} & 0 \text{ samples} & 0 \text{ samples} \\ 0 \text{ samples} & 0 \text{ samples} & 0 \text{ samples} \\ 0 \text{ samples} & 0 \text{ samples} & 0 \text{ samples} \end{bmatrix}. \tag{23}$$

4.5. Scenario 2 — Full mismatch diagnosis

To determine the effectiveness of the PMR in diagnosing MPM within all parameters of the transfer function matrix in (17), the second simulation includes the full uncertainty description of (20) as MPM.

4.5.1. Step 1 — Gain mismatch

The MPM for the gain terms can be obtained from the zero-frequency components of the PMR as seen in Fig. 7.

$$\begin{aligned} \Delta K &= \left(|\mathbf{G_{PMR}}(0)| - 1\right) \times 100 \\ &= \left(\begin{bmatrix} 0.0605 & 1.1929 & 0.4397 \\ 2.0237 & 1.1567 & 1.3768 \\ 1 & 1 & 1 \end{bmatrix} - 1\right) \times 100 \\ &= \begin{bmatrix} -93.95\% & 19.29\% & -56.03\% \\ 102.37\% & 15.67\% & 37.68\% \\ 0\% & 0\% & 0\% \end{bmatrix}. \end{aligned} \tag{24}$$

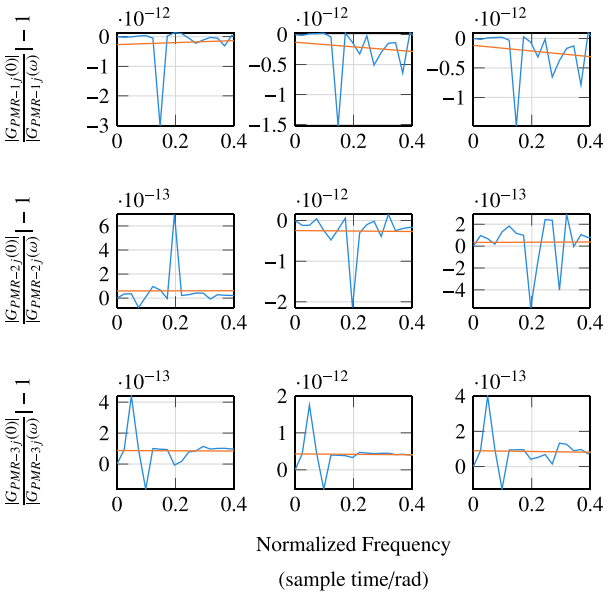

Fig. 5. Initial slope of PMR magnitude spectra for Scenario 1. (For interpretation of the references to color in this figure legend, the reader is referred to the web version of this article.)

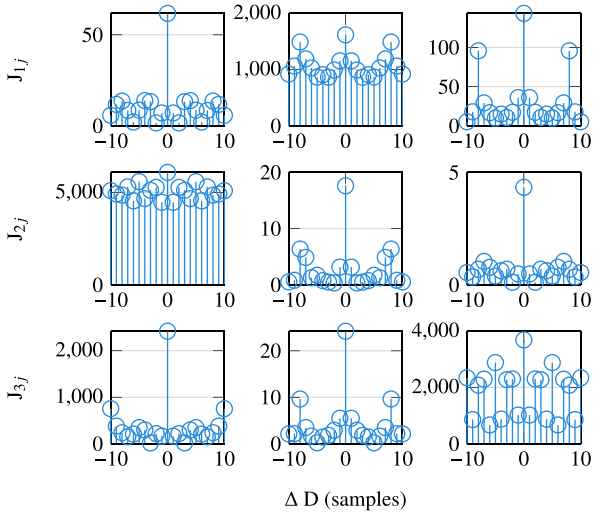

Fig. 6. Objective function results for Scenario 1.

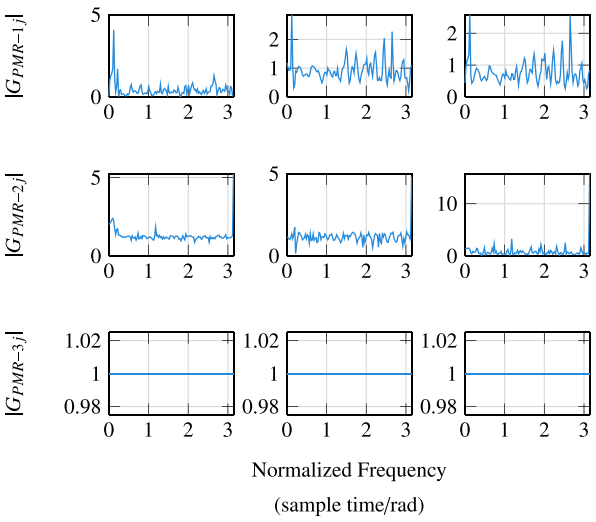

Fig. 7. PMR magnitude spectra for Scenario 2.

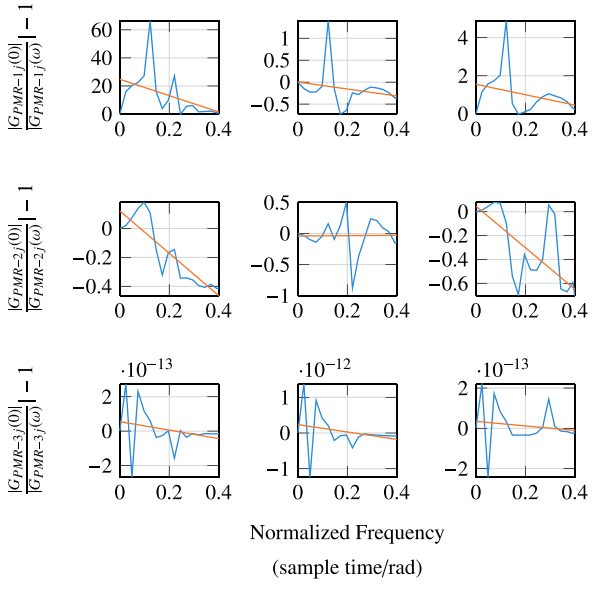

Fig. 8. Initial slope of PMR magnitude spectra for Scenario 2.

4.5.2. Step 2 — Time-constant mismatch

The relative time-constant mismatches can be deduced from the linear fitted line (orange line) to the initial slope of the PMR magnitude spectrum as seen in Fig. 8.

$$\Delta\tau = \hat{\alpha}_{\mathbf{G_{PMR}}} \times -100 = \begin{bmatrix} 5.819 & 0.079 & 0.273 \\ 0.147 & -0.0029 & 0.174 \\ 0 & 0 & 0 \end{bmatrix} \times 10^3. \tag{25}$$

4.5.3. Step 3 — Delay mismatch

The results of the cost function, used for the optimal delay estimation, are visible in Fig. 9.

$$\Delta D = \begin{bmatrix} 6 \text{ samples} & 0 \text{ samples} & 0 \text{ samples} \\ 0 \text{ samples} & 0 \text{ samples} & -1 \text{ samples} \\ 0 \text{ samples} & 0 \text{ samples} & 0 \text{ samples} \end{bmatrix}. \tag{26}$$

4.6. Scenario 3 — Grindcurve detection using the PMR

The parabolic relationships between the throughput, grind, and power of a grinding mill in terms of the mill load are called grind curves (Powell et al., 2009; Le Roux et al., 2020). Depending on the operating conditions of the grinding mill, it is possible to operate either to the left or right of the peak in a grind curve. The process dynamics may invert when the process crosses a peak. The aim of Scenario 3 is to simulate the crossing of the peak in the grind curves of the mill by inverting the signs of G_{11} and G_{22}. Along with the sign changes, the full uncertainty description of (20) is also applied to the mill.

The MPM diagnosis presents the same results as in (24)–(26). This is expected, as the change in sign of G_{11} and G_{22} does not influence the magnitude of the process gain, time constants, or time delays. However, the sign change influences the phase spectrum of the PMR as described in (2). The analysis of the phase spectrum is shown in Fig. 10.

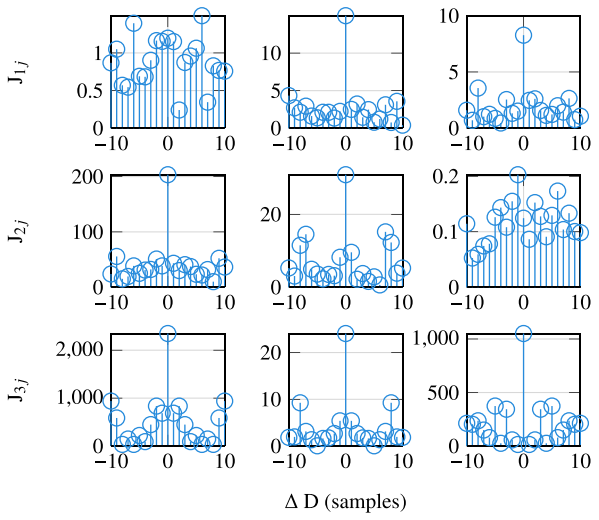

Fig. 9. Objective function results for Scenario 2.

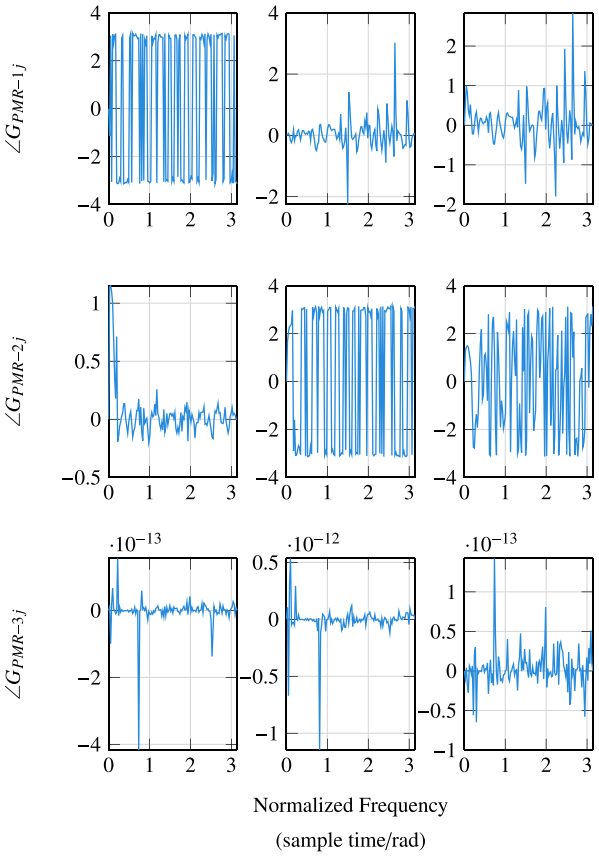

Fig. 10. PMR phase spectra for Scenario 3.

5. Discussion of results

5.1. Scenario 1 results

For Scenario 1, from (21), (22), and (23) it is evident that the PMR can identify the MPM for all parameters given that only a gain mismatch is present in the system. However, this may be unrealistic as some mismatch is normally present in the other parameters as well.

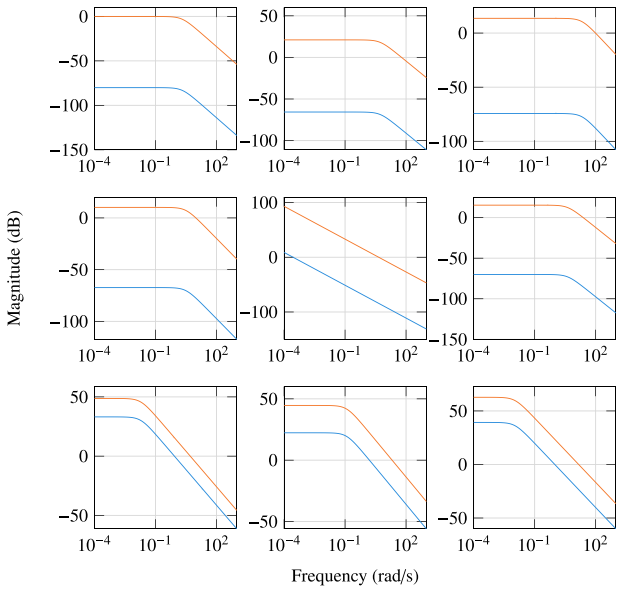

Fig. 11. Bode magnitude of G and G_{scaled}. (For interpretation of the references to color in this figure legend, the reader is referred to the web version of this article.)

5.2. Scenario 2 results

From (24), (25), and (26) it is evident that if all the parameters experience mismatches, the PMR is unable to correctly diagnose MPM for a grinding mill represented by a multivariable transfer function matrix.

Recall that the PMR can be expanded to a polar representation,

$$G_{PMR}(e^{j\omega}) = \frac{|G(e^{j\omega})|e^{j\angle \underline{G}(e^{j\omega})}e^{-jD\omega}}{|\hat{G}(e^{j\omega})|e^{j\angle \underline{\hat{G}}(e^{j\omega})}e^{-j\hat{D}\omega}}. \tag{27}$$

This polar representation of the PMR reveals that both the magnitude spectrum as well as the phase spectrum are influenced by a time-constant mismatch. Furthermore, as discussed in Section 2.1, the time-constant mismatch diagnosis consists of a linearity check on the rate of change of the PMR magnitude spectrum. Therefore, if certain models within the MIMO transfer function have faster dynamics when compared to other transfer functions, some frequency-based information might be filtered out, rendering the PMR less effective.

It should be noted that the PMR is developed for FOPTD systems. (17) contains a pure integrator, instead of fully consisting of FOPTD transfer functions. This does not pose a problem seeing that the PMR was developed to identify the MPM, without any knowledge of the system, under the assumption that all models of the system are FOPTD. Since the PMR is an offline method and has no effect on the closed-loop performance of the system, the PMR can accommodate pure integrators, which are interpreted as FOPTD models with the dynamics orders of magnitude magnitudes slower than the other models in the system.

Fig. 11 shows a Bode magnitude plot of the unscaled plant model in (17) (blue line) and the scaled plant model in (19) (orange line). The dynamic imbalance in the plant can be observed by inspecting the role-off rate rates and the critical frequencies. The dynamic imbalances within the plant can be seen between for example G_{22} and G_{12} or G_{11} and G_{31}. These dynamic imbalances will cause certain parts of the plant to react faster to the setpoint changes than others, causing a filtering effect on frequency-based information.

5.3. Scenario 3 results

The effects that the time-constant and delay mismatches have on the phase spectrum, as defined in (2), are visible within all plots of

Fig. 10. However, the rapid phase wrapping about $\pm\pi$ is clearly visible for $\angle G_{PMR-11}$ and $\angle G_{PMR-22}$. This leads to the identification of the sign change for G_{11} and G_{22} in the presence of MPM.

In the case where a process disturbance causes the peaks of the grind curve to shift such that the process operates to the right of the peak, the change in the direction of the response can be identified by evaluating the phase spectrum of the PMR. Early identification of a change in the operating conditions of the plant may help operators to quickly adapt to these changes.

6. Conclusion

The PMR can be a helpful tool for process engineers to detect MPM and diagnose controllers that are performing sub-optimally. This is especially true for SISO system as shown in Yerramilli and Tangirala (2018). The PMR method works very well to identify gain mismatches, but only if the dynamics of the model (as represented by the time constant of the model) closely match the dynamics of the process (Scenario 1). If there is a large mismatch in dynamics represented by time constant parameters as shown in Scenario 2, the PMR is unable to accurately capture the MPM present in the grinding mill. This is a result of a filtering effect of the fast components in the model. However, in general, a controller is capable of controlling the plant as long as the direction of change between variables is captured correctly. In this case, the PMR is a helpful tool to identify a change in the direction.

Future work will consider quantifying the point at which dynamic imbalance causes the PMR to misidentify MPM. In addition, consideration will be given to decoupling the system in terms of slow and fast dynamics before applying the PMR.

CRediT authorship contribution statement

Heinz K. Mittermaier: Writing – review & editing, Writing – original draft, Visualization, Validation, Software, Methodology, Investigation, Formal analysis, Conceptualization. **Johan D. le Roux:** Writing – review & editing, Supervision, Resources, Conceptualization. **Ian K. Craig:** Writing – review & editing, Supervision, Resources.

Declaration of competing interest

The authors declare the following financial interests/personal relationships which may be considered as potential competing interests: J.D. Le Roux reports financial support was provided by National Research Foundation of South Africa. If there are other authors, they declare that they have no known competing financial interests or personal relationships that could have appeared to influence the work reported in this paper.

Acknowledgments

This work is based on the research supported in part by the National Research Foundation of South Africa (Grant Number: 137769).

Data availability

No data was used for the research described in the article.

References

Badwe, A.S., Gudi, R.D., Patwardhan, R.S., Shah, S.L., Patwardhan, S.C., 2009. Detection of model-plant mismatch in MPC applications. J. Process. Control 19 (8), 1305–1313.

Coetzee, L.C., Craig, I.K., Kerrigan, E.C., 2010. Robust nonlinear model predictive control of a run-of-mine ore milling circuit. IEEE Trans. Control Syst. T. 18 (1), 222–229.

Craig, I.K., Hulbert, D.G., Metzer, G., Moult, S.P., 1992. Optimised multivariable control of an industrial run-of-mine milling circuit. J. S. Afr. Inst. Min. Met. 92 (6), 169–176.

Craig, I.K., MacLeod, I.M., 1995. Specification framework for robust control of a run-of-mine ore milling circuit. Control Eng. Pract. 3 (5), 621–630.

Hamon, B.V., Hannan, E.J., 1974. Spectral estimation of time delay for dispersive and non-dispersive systems. J. R. Stat. Soc. C-Appl. 23 (2), 134–142.

Hodouin, D., 2011. Methods for automatic control, observation, and optimization in mineral processing plants. J. Process. Control 21 (2), 211–225.

Lathi, B.P., Ding, Z., 2010. Modern Digital and Analog Communication Systems, fourth ed. In: The Oxford Series in Electrical and Computer Engineering, Oxford University Press.

Le Roux, J.D., Craig, I.K., 2019. Plant-wide control framework for a grinding mill circuit. Ind. Eng. Chem. Res. 58 (26), 11585–11600.

Le Roux, J.D., Steinboeck, A., Kugi, A., Craig, I.K., 2020. Steady-state and dynamic simulation of a grinding mill using grind curves. Min. Eng. 152, 106208.

Le Roux, J.D., Steyn, C.W., 2022. Validation of a dynamic non-linear grinding circuit model for process control. Min. Eng. 187, 107780.

Li, L., Lu, L., Huang, Z., Chen, X., Yang, S., 2020. A model mismatch assessment method of MPC by decussation. ISA Trans. 106, 51–60.

Lindemann, M., Raethjen, J., Timmer, J., Deuschl, G., Pfister, G., 2001. Delay estimation for cortico-peripheral relations. J. Process. Control 111 (2), 127–139.

Ljung, L., 1999. System Identification: Theory for the User, second ed. In: Prentice Hall Information and System Sciences Series, Prentice Hall PTR, Upper Saddle River, NJ.

Mayne, D.Q., 2014. Model predictive control: Recent developments and future promise. Automatica 50 (12), 2967–2986.

Mittermaier, H.K., Le Roux, J.D., Olivier, L.E., Craig, I.K., 2023. Model-plant mismatch detection for a plant under Model Predictive Control: A grinding mill circuit case study. IFAC- Pap. 56 (2), 11778–11783.

Morrell, S., Finch, W., Kojovic, T., Delboni, H., 1996. Modelling and simulation of large diameter autogeneous and semi-autogeneous mills. Int. J. Miner. Process. 44–45, 289–300.

Olivier, L.E., Craig, I.K., 2013. Model-plant mismatch detection and model update for a run-of-mine ore milling circuit under model predictive control. J. Process. Control 23 (2), 100–107.

Olivier, L.E., Craig, I.K., 2017. A survey on the degree of automation in the mineral processing industry. In: 2017 IEEE AFRICON. pp. 404–409.

Oppenheim, A.V., 1999. Discrete-Time Signal Processing. Pearson Education, India.

Pomerleau, A., Hodouin, D., Desbiens, A., Gagnon, É., 2000. A survey of grinding circuit control methods: From decentralized PID controllers to multivariable predictive controllers. Powder Technol. 108 (2–3), 103–115.

Powell, M., Van Der Westhuizen, A., Mainza, A., 2009. Applying grindcurves to mill operation and optimisation. Min. Eng. 22 (7–8), 625–632.

Priestley, M.B., 1981. Spectral Analysis and Time Series. Academic Press, London; New York, v. 1. Univariate series.– v. 2. Multivariate series, prediction and control.

Proakis, J.G., Salehi, M., 2014. Fundamentals of Communication Systems, second ed. Pearson, Boston.

Qin, S., Badgwell, T.A., 2003. A survey of industrial model predictive control technology. Control Eng. Pract. 11 (7), 733–764.

Ramasamy, M., Narayanan, S., Rao, C.D.P., 2005. Control of ball mill grinding circuit using model predictive control scheme. J. Process. Control 15 (3), 273–283.

Remes, A., Aaltonen, J., Koivo, H., 2010. Grinding circuit modeling and simulation of particle size control at Siilinjärvi concentrator. Int. J. Miner. Process. 96 (1–4), 70–78.

Schwenzer, M., Ay, M., Bergs, T., Abel, D., 2021. Review on model predictive control: An engineering perspective. Int. J. Adv. Manuf. Technol. 117 (5), 1327–1349.

Selvanathan, S., Tangirala, A.K., 2010a. Diagnosis of poor control loop performance due to model-plant mismatch. Ind. Eng. Chem. Res. 49 (9), 4210–4229.

Selvanathan, S., Tangirala, A.K., 2010b. Time-delay estimation in multivariate systems using Hilbert transform relation and partial coherence functions. Chem. Eng. Sci. 65 (2), 660–674.

Skogestad, S., Postlethwaite, I., 2010. Multivariable feedback control: Analysis and design, second ed. Wiley, Chichester.

Steyn, C.W., Brooks, K.S., De Villiers, P.G.R., Muller, D., Humphries, G., 2010. A holistic approach to control and optimization of an industrial run-of-mine ball milling circuit. IFAC- Pap. 43 (9), 137–141.

Wei, D., Craig, I.K., 2009. Grinding mill circuits — A survey of control and economic concerns. Int. J. Miner. Process. 90 (1–4), 56–66.

Wu, Q., Du, W., 2022. Online detection of model-plant mismatch in closed-loop systems with Gaussian processes. IEEE Trans. Ind. Inf. 18 (4), 2213–2222.

Yerramilli, S., Tangirala, A.K., 2016. Detection and diagnosis of model-plant mismatch in MIMO systems using plant-model ratio. IFAC- Pap. 49 (1), 266–271.
Yerramilli, S., Tangirala, A.K., 2018. Detection and diagnosis of model-plant mismatch in multivariable model-based control schemes. J. Process. Control 66, 84–97.
Ziolkowski, L., Le Roux, J.D., Craig, I.K., 2022. Extremum seeking control for optimization of an open-loop grinding mill using grind curves. J. Process. Control 114, 54–70.
Zou, H., 2006. The adaptive Lasso and its oracle properties. J. Amer. Statist. Assoc. 101 (476), 1418–1429.